MAGNETIC FLUX ROPES AS MODELS OF A SOLAR FLARE AND TRANSITION OF FLARE FILAMENT INTO CMI-REGIM OF MOTION

© 2025 A. A. Solov'ev, O. A. Korolkova, E. A. Kirichek

Central (Pulkovo) Astronomical Observatory of RAS, St. Petersburg, Russia

**e-mail: solov@gaoran.ru*

***e-mail:korolkova@gaoran.ru*

****e-mail: elenakirichek@gmail.com*

Received February 01, 2025

Revised March 19, 2025

Accepted April 14, 2025

Abstract. A new physical mechanism of flare energy release in force-free magnetic flux ropes is described: as the top of the magnetic rope-loop enters the corona, the external pressure G, which keeps it from expanding, steadily decreases. At its critically low value, the longitudinal field tends to zero on the magnetic surface where the currents change sign, and the force-free parameter and azimuthal current near this surface grow without limit, approaching the rupture. This excites plasma turbulence in the rope and serves as a flare trigger. Rapid dissipation of the field and currents on the anomalous plasma resistance induces an electric field much higher than the Dreiser field. The forces acting on the flare filament in the corona are described, and the conditions for its transition to the dynamic CME regime are discussed.

Keywords: *solar flare, magnetic field, force-free magnetic flux rope, plasma instability, equilibrium of filament, coronal mass ejection*

DOI: 10.31857/S00167940250401e8

1. INTRODUCTION

Solar flares are the most powerful and impressive manifestation of solar activity, but, at the same time, they present the greatest difficulties for its understanding and theoretical interpretation. It is generally accepted that a flare event is the result of annihilation of magnetic energy, when a contact of strong magnetic fields of different polarity occurs in the active region of the Sun in the presence of a topologically complex magnetic configuration. Of course, in such a situation, the release of some part of magnetic energy in the emerging current layers is inevitable. There is even a "standard" model of a flare [see, e.g., Priest 1982; Chen et al. 2020 and references there]; a great number of papers [Priest, Forbes 2000; Kadomtsev 1979, and many others] are devoted to the theoretical description of the process of reconnection of magnetic lines of force. Some observed flare phenomena are not badly described within the framework of such representations. There are, however, serious difficulties. The point is that the current layer, in which the reconnections of magnetic lines of force should occur, turns out to be extremely unstable with respect to hydrodynamic turbulence, which rapidly transforms it into a mixture of small-scale magnetic islands and hot spots whose sizes, intensities, and positions change rapidly and chaotically. Such a picture of the destruction of magnetic surfaces is presented, in particular, in Artsimovich and Sagdeev [1979]. The complex character of reconnection of magnetic force lines is also widely presented in the well-known monograph [Priest and Forbes, 2000]. Chaotization of the internal structure of the layer disrupts the regular lateral flow of external field fluxes into it and does not allow one to accurately calculate the amount of magnetic energy entering the layer, as well as the amount and energy of particles accelerated in it.

A major contribution to understanding the physical nature of outbursts was made by Fleishman et al. [2020, 2022]. They show on the basis of radio observations that a flare is energized not by the inflow of an external field, but by the reduction of the energy of its internal magnetic field in the region of energy release (*in situ*). Based on these works, we attempt to extend the existing understanding of the mechanisms of flare energy release by showing that it can be quite effective in individual twisted magnetic loops (bundles) when the electric current density in them is high enough to excite plasma instability and the appearance of "anomalous resistance". There is a large number of observations in the radio, UV and X-ray ranges of so-called flare loops, where signs of reconnection of magnetic force lines are not recorded, but flare energy release in them takes place. For example, a powerful class X solar flare observed on the 1.6-m *New Solar Telescope* in a single twisted magnetic fiber, [Wang et al., 2015], showed no signs of magnetic reconnection. An example of a strong flare in a single twisted magnetic fiber is also the X1 class flare recorded at the

Solar Dynamics Observatory on 22.09. 2011. It was characterized by a very long (about 12 hours) energy release due to the continuous transfer of the azimuthal field from the legs of the long magnetic loop to the region of the flare energy release, where the critical current density was reached [Solov'ev and Murawski, 2014]. In general, it should be noted that in the vast majority of cases, the flare loops observed in various ranges of the solar spectrum have a regular rounded shape at their tops without signs of its distortions such as helmet-shaped structures that would indicate external injection of charged particles or reconnections. These images of flash loops create a clear impression that the energy release observed in them is caused not by an external influence, not by contact with a field of a different sign, but by an internal stock of free magnetic energy accumulated in a sufficiently strongly twisted magnetic field of the loop itself. Proceeding from all of the above, in recent years we have been developing models of solar flares that can occur in forceless magnetic harnesses - in weakly twisted twisted magnetic force tubes possessing a sufficient stock of free magnetic energy stored in the currents flowing in them. The structure of this paper is as follows: in Section 2, we briefly recall the main properties of magnetic bundles in the highly conducting solar corona: the shielding of electric currents, the presence of external pressure keeping the bundle from lateral expansion, and the forceless nature of the magnetic field in the bundle. In Section 3, we instantiate the internal magnetic and current structure of the harness using two different flux functions, one specifying the concentration of currents at the axis of the harness and the other in its thin peripheral shell. In Section 4, we also very briefly outline the flare mechanism in the bundle and in Section 5 we proceed to analyze the forces acting on the flashed fiber and the conditions for its transition to the coronal mass ejection (CME) regime. In Section 6, we compare this analysis with observations and conclude that it adequately reflects reality.

The aim of this paper is to provide a rationale for their observed dynamics by recalling the basic properties of magnetic bundles and the mechanism of flash energy release in them.

2. BASIC PROPERTIES OF MAGNETIC BUNDLES IN PLASMA

The main property distinguishing magnetic bundles in a conducting medium (plasma) from currents in vacuum (or in air) is that the total electric current along the axis of such a bundle is strictly equal to zero (Fig. 1). This property - shielding of the current within the MHD framework has long been well realized and discussed in detail [Parker 1979, 2007; Kadomtsev 1979; Solov'ev and Kirichek, 2021], although the number of amateurs using simple formulas for unshielded currents from the course of general physics, unfortunately, is not decreasing.

Fig. 1.

The second most important property of bundles in plasma is that they all have a finite transverse size and need for their lateral equilibrium an external pressure that would keep them

from infinite expansion. In the rarefied solar corona, the role of such a factor is played by the external magnetic field (Fig. 1).

Since a sufficiently high (at least 100 Gs) magnetic field strength is needed to produce even a small flare, and the gas pressure in the corona corresponds to a magnetic field pressure of 1 Gs, we can state with a high degree of accuracy that the magnetic field structure of the flare bundle is forceless, i.e., its magnetic field is described by Eqs:

$$[\nabla \times \boldsymbol{B}] = \alpha(\boldsymbol{r})\boldsymbol{B},\ \nabla\alpha(\boldsymbol{r}) \cdot \boldsymbol{B} = 0 \quad , (1)$$

where $\alpha(r)$ is some pseudoscalar function, the square of the value of which determines the Joule dissipation rate of the forceless field. We consider the equilibrium of a horizontal magnetic fiber in a flat hydrostatic atmosphere in the presence of a homogeneous gravity field and an external magnetic field longitudinal to the fiber axis. The radius of the fiber cross section is always a finite value, so that at its boundary, at $r =$ a, the azimuthal magnetic field tends to zero: $B_{\varphi}(ka) \to 0$, and the longitudinal field passes into an external longitudinal field that protects the bundle from expanding to infinity: $B_z(ka) \to B_{z,ex}$ (Fig. 1). We assume axial and translational symmetry - invariance of the system parameters with respect to arbitrary displacements along one of the coordinates. Let this be the z-axis in Cartesian coordinates, as in the cylindrical model of Parker [1979], the axis is directed across the fiber, and the *y-axis is* directed vertically upward. The *y* distances are counted upward from the magnetic axis of the fiber. The force of gravity will be $\boldsymbol{F}_g = -\rho(y)g\boldsymbol{e}_y$, where ρ is the gas density, and the equations of magnetic hydrostatics will take the form

$$(4\pi)^{-1}\left[[\nabla \times \boldsymbol{B}] \times \boldsymbol{B}\right] - \nabla P - \rho g \boldsymbol{e}_y = 0, \qquad (2)$$

$$div\boldsymbol{B} = 0, \qquad (3)$$

$$P = \rho \Re T \mu^{-1}. \qquad (4)$$

Here $\boldsymbol{B}$ is the magnetic field strength, P is the pressure, and T the gas temperature, μ is the average molar mass of the gas. Equation (2) gives the balance of forces in the equilibrium system, equation (3) determines the solenoidal character of the magnetic field, and (4) gives the state of an ideal gas. The system (2) - (4) is incomplete: it lacks the energy transfer equation, but this does not matter when considering strong force-free fields, when the pressure gradient, like all other forces, is discarded. Our problem is to find that equilibrium state of the fiber when such physical conditions develop in it that plasma turbulence can begin and anomalous plasma resistance can arise. With the

onset of such a process, the approximation of magnetic statics is no longer valid, and we must use the MHD induction equation, which contains time in explicit form, to describe the flash energy release. A remarkable property of forceless magnetic fields is that at Joule dissipation their internal structure does not change, only their amplitude decreases, so we do not have to search for a new equilibrium of the system.

It is convenient to describe the magnetic field in a fiber by a flux function [Landau and Lifshitz, 1984]:

$$A(x,y)=\int_0^x B_y(x,y)dx. \qquad (5)$$

The components of the azimuthal field are given, according to condition (3), by the formulas:

$$B_y=\frac{\partial A}{\partial x},\quad B_x=-\frac{\partial A}{\partial y}. \qquad (6)$$

The equilibrium equation (2) with the help of the flux function can be rewritten as follows [Solov'ev 2022]:

$$\frac{\partial^2 A(x,y)}{\partial x^2}+\frac{\partial^2 A(x,y)}{\partial y^2}=-\frac{1}{2}\frac{dB_z^2(A)}{dA}-4\pi\frac{\partial P(A,y)}{\partial A}\ . \qquad (7)$$

Hence, specifying the flux function and discarding the gas pressure term, we obtain the equation for finding the longitudinal magnetic field, which, by virtue of translational symmetry, appears to depend only on the function A.

3. STRUCTURE OF THE MAGNETIC FIELD IN A FORCELESS HARNESS

In this paper, we consider two flow functions:

$$A_1=\frac{B_0}{k}\exp\left(-(k^2x^2+k^2y^2-1)\right)=\frac{B_0}{k}\exp\left(-(k^2r^2-1)\right) \qquad (8)$$

$$A_2=\frac{B_0}{k}\exp\left(\frac{-1}{m(k^2x^2+k^2y^2-1)}\right)=\frac{B_0}{k}\exp\left(\frac{-1}{m(k^2r^2-1)}\right) \qquad (9)$$

Here m = 1, 2, 3..., $kr=\sqrt{x^2+y^2}$. The first of these functions, a decreasing exponent, describes a bundle with a strong concentration of longitudinal current on the axis (Fig. 1, left, and Fig. 3), while the second (called a "cap") sets a sharp current maximum at the periphery, in a thin cylindrical shell; the larger the index m, the sharper the peak current concentration in this shell (Fig. 1, right, and Fig. 4).

For the first model, the calculation of the longitudinal magnetic field in the harness using the above algorithm gives:

$$B_z(r) = B_0\sqrt{G - 2\cdot\left(\exp(k^2r^2-1)\right)^{-2}\cdot\left[1-2\ln\left(\exp(k^2r^2-1)\right)^{-1}\right]} \qquad (10)$$

where $G = B_{z,ex}^2 B_0^{-2}$ is the integration constant. Its critical value, at which the substring expression turns to zero on the current sign change surface, is equal to 2 (Fig. 2).

For the second model (cap) for the case $m = 2$, we obtain

$$\frac{B_z(r)}{B_0} = \left\{G - \left[\exp\left(\frac{-1}{2\left(1-k^2r^2\right)}\right)\right]^2\cdot\left[\frac{-1}{(k^2r^2-1)^2}+\frac{2}{k^2r^2-1}-2+\frac{1}{(k^2r^2-1)^3}+\frac{1}{(k^2r^2-1)^4}\right]\right\}^{\frac{1}{2}} \qquad (11)$$

$G = B_{z,ex}^2 B_0^{-2}$, the value of the integration constant at which the longitudinal field goes to zero at the current sign change surface is here . $G_{cr=} = 3.1974$

Fig. 2.

Fig. 3.

Fig. 4.

4. FLASH MECHANISM IN A FORCELESS MAGNETIC HARNESS

In the harness models of solar flare that we develop, we reveal a new physical mechanism of flare energy release in forceless magnetic harnesses.

Its essence is as follows: as the top of the magnetic loop-bundle exits into the solar corona, the external pressure G, which keeps the bundle from lateral expansion, will steadily fall. It turns out that for any forceless bundle, regardless of its internal magnetic structure, there is a critically low value of this external pressure at which the longitudinal magnetic field tends to zero at the magnetic surface where the electric currents change sign. (This *CIS* is the *current inversion surface*). (Figure 5 demonstrates this effect for the second model with m = 2.) When $B_z(CIS) \to 0$, the azimuthal electric current $j_\varphi(kr)$ and the powerless parameter $\alpha(kr)$ begin to increase unboundedly (modulo) in the neighborhood of this surface, approaching a discontinuity of the second kind. At that, the current (drift) velocity of electrons near the *CIS* surface will inevitably exceed the ionic sound velocity.

Fig. 5.

This will cause excitation of plasma ion-sonic instability in the bundle.

The scattering of current electrons on ionic sound plasmons very sharply, by 6-7 orders of magnitude, lowers the plasma conductivity [Artsimovich and Sagdeev, 1979; Kaplan and

Tsytovich, 1973]. At such an anomalously high resistance, the harness plasma is strongly heated, the magnetic field dissipates rapidly, and the rate of decrease of its strength reaches several Gauss/second [Fleishman et al., 2020, 2022]. According to Faraday's law of induction, this generates powerful electric fields in the harness that are much larger than the Dracer field. The aggregate of the described phenomena well reflects the nature of flare events.

As can be seen from the above two models, despite the sharp difference in the distributions of electric currents along the cross section of the fiber, the basic properties of the forceless magnetic bundle, which ensure the flash energy release in it, are fully preserved. A description of the flare bundle models is given in a number of our recent papers [Solov'ev and Kirichek, 2021, 2023; Solov'ev, 2022, 2024, etc.], so here we will not dwell on the analysis and proof of the above statements, but will turn to the question of what forces act in the rarefied solar corona on the flare fiber and under what conditions it can transition from equilibrium to the dynamic CME regime.

5. FORCES ACTING ON THE FLASH FIBER

Let us first consider the internal forces in a straight magnetic cylinder of radius a , length L with two field components: $B_z(r), B_\varphi(r)$. We will consider the quantities averaged over the cross-section of the harness (we use angle brackets $\langle\ \rangle$). First of all, we note that the transverse equilibrium condition for a forceless magnetic bundle has the form: $\left\langle B_z^2 \right\rangle = B_{z,ex}^2$ [e.g., Solov′ ev, 2021], so that the azimuthal field does not enter this balance due to the shielding of the currents. As for the equilibrium of the harness in length, the tension of the longitudinal field $-\left\langle B_z^2 \right\rangle (4\pi)^{-1}$ tends to shorten the harness in length, while the mutual repulsion of the azimuthal field rings strung on a common magnetic axis, on the contrary, stretches the harness in length: $+\left\langle B_\varphi^2 \right\rangle (8\pi)^{-1}$. The balance of these internal forces is such that if we introduce an integral torsion of the field by the ratio $\kappa = \left\langle B_\varphi^2 \right\rangle \left\langle B_z^{-2} \right\rangle$, the equilibrium of the magnetic bundle along its length occurs at $\kappa = 2$ [Parker,1979]. At smaller values of torsion the tourniquet will shrink, reducing its length, and at larger values it will elongate, stretching out. The internal force acting per unit length of the tourniquet will be written in the form

$$F_L(\text{int}) = \frac{V}{L}\frac{\left\langle B_z^2 \right\rangle}{8\pi}(\kappa - 2) \qquad (12)$$

However, this simple picture is disturbed by the fact that in addition to the mentioned internal forces, external forces will act on the magnetic fiber. The first of them is related to the fact that the longitudinal magnetic field, which keeps the bundle from lateral expansion to infinity, being a part of the general large-scale magnetic field, can noticeably change on the scale of the bundle cross-

section *a*. We cannot measure or calculate this change in each observed case. Neither we can measure nor calculate this change in each observed case. We can only conclude from general considerations that the pressure of this field must fall with height, and thus, a positive external force equal in order of to the following must act on the bundle

$$F_{L,1}(external) = V\frac{d}{dh}(\frac{B_{z,ex}^2}{8\pi}) \approx \frac{V}{a}\frac{B_{z,ex}^2}{8\pi} = \frac{V}{a}\frac{\left\langle B_z^2 \right\rangle}{8\pi}. \quad (13)$$

This force is positive and noticeably larger than (12), since in it L is replaced by a, while the length of the loop is usually much larger than its cross-sectional radius.

The second external force is due to the presence of an external magnetic field **transverse** to the magnetic axis of the harness. Two cases should be distinguished here:

Fig. 6.

1. If the direction of the external transverse field coincides with the direction of the azimuthal field at the lower bypass of the bundle, there is a positive force supporting the bundle from bottom to top (Fig. 6), and in sum with (13), this will provide fiber lifting and CME formation immediately after the flash or simultaneously with it, which is often observed.

2. If the transverse field coincides with B_φ on the upper bypass of the bundle, there is an overlap of the fiber with a "magnetic dome" that prevents its upward movement (Fig. 7). The force due to this field will be:

$$F_{L,2}(external) = -\frac{V}{a}\frac{B_{ex}^2}{8\pi}\sin(\mu), \quad (14)$$

where μ is the angle between the direction of the vector $\mathbf{B}_{ex}$ and the magnetic axis of the harness. The competition of two differently directed external forces (13) and (14) will determine the whole dynamics of the magnetic bundle.

As already mentioned, unfortunately, we cannot measure or calculate these external forces, and only from the reconstruction of the forceless magnetic field in the corona [Bakunina et al. 2024] we can estimate the angle μ . In those cases when it is small, i.e., when the fiber bundle is placed almost parallel to the external field, the braking effect of the transverse field is weakened, and then the fiber can go from equilibrium to the CWM regime and in case 2, i.e., even in the presence of weak transverse overlap with the external field

Fig. 7.

The trajectory of further movement of the fiber depends on whether the external magnetic field has a so-called "shire", i.e., whether the angle between the fiber axis and the external field changes with height. If such a change in the orientation of the external field takes place, and it turns

out to be such that its transverse component will be growing, raked by the rising fiber and due to this amplification, then, eventually, the fiber lifting will be stopped and it can collapse back to the photosphere. This is the so-called *failed ejection*. A vivid example of such an event is presented, for example, in [Ji et al., 2003].

If the fiber rises to the so-called source surface, where the external magnetic field becomes radial, the further dynamics of such a magnetic bundle will be determined not only by the internal force (12), but also by its interaction with the solar wind flow

6. COMPARISON OF THEORY WITH OBSERVATIONS

In recent years, the concept of *magnetic flux ropes* as the main fl*are* structures on the Sun has received strong observational support in the works of V.F. Melnikov's group [Bakunina et al., 2024]. In nonlinear 3D reconstructions of forceless magnetic fields in flare-active regions, they invariably find powerful current structures (with currents up to 10^{13} Ampere) in the form of twisted magnetic force tubes (bundles), which serve as bright sources of both microwave and extreme ultraviolet radiation. The analysis of the connection between the flash energy release and the transition of the fiber to the CME mode has shown, in full accordance with the above theoretical considerations, that in those cases when the fiber is blocked by a powerful magnetic dome, the flash is not accompanied by the appearance of the CME. The emission is formed only in those cases when the external field is very weak or when the axis of the flashed fiber is located almost parallel to the direction of the external field. In this case, the fiber, slightly twisted, can relatively easily slip between the magnetic force lines of this external field and "escape into the breakaway". Of course, when the flare fiber penetrates through the external fields, which can have a complex entangled structure, often at the periphery of the magnetic fiber there are contacts of fields of opposite sign, and then there are reconnections of magnetic force lines, which noticeably complicate, but, at the same time, and enrich this flare phenomenon. The internal structure of the magnetic bundle in these processes can undergo significant transformations, as presented in [Melnikov and Meshalkina, 2024], but here, too, the dynamics of the powerful magnetic bundle as the main source of free magnetic energy remains the basis of the flash event.

7. CONCLUSIONS

1. The harness models of solar flare energy release rely not on the mechanism of reconnection of magnetic force lines, which is practically incalculable, but on the intrinsic physical properties inherent in all forceless harnesses, regardless of their internal current structure. Electric currents may concentrate on the axis of the magnetic harness or in its peripheral shell, but when the external pressure that keeps the harness from laterally expanding to infinity as the top of the twisted magnetic loop emerges into the corona drops to some critically small value, a parametric

catastrophe occurs in the harness. The longitudinal magnetic field tends to zero at that magnetic surface where the currents change sign, and the azimuthal electric current density and the powerless parameter begin to increase unboundedly near that surface. In such a situation, the current (drift) velocity of electrons will inevitably exceed in the vicinity of this magnetic surface the ion sound velocity, which will lead to the excitation of plasma instability in the bundle with all the ensuing consequences.

2 The analysis of the forces acting on the flash fiber shows that its dynamics is largely determined by the structure and strength of the magnetic field external to the fiber. The structure of this external field is not available to us from observations, but it can be theoretically reconstructed in the nonlinear force-free approximation from photospheric magnetograms. In this case, we can draw certain conclusions about the possible transition of the flashed forceless fiber from quasi-equilibrium to the dynamical KVM regime. The available experience in the reconstruction of magnetic fields in the corona shows that flagellar forceless structures are the most typical flare configurations on the Sun, and in this respect flagellar flare models are highly relevant.

FUNDING

The work was performed within the framework of the State Assignment of the Main (Pulkovo) Astronomical Observatory of the Russian Academy of Sciences.

CONFLICT OF INTERESTS

The authors declare that there is no conflict of interest.

REFERENCES

1. *P. A. Artsimovich, R. Sagdeev. 3.* Plasma Physics for Physicists. Moscow: Atomizdat. 278 c. 1979.

2. *Bakunina, I.A.; Melnikov, V.F.; Shain, A.V.; Kuznetsov, S.A.; Abramov-Maksimov, V.E.* Microwave radiation behavior in active regions with "locked" and "open" magnetic bundles / Proceedings of the 28th All-Russian Conference "Solar and Solar-Terrestrial Physics". SPb. GAO RAS. October 7-11, 2024. C. 25–28. doi.org/10.31725/0552-5829-2024-25-28

3. *Kadomtsev V.V.* Closure of force lines in magnetic hydrodynamics // "Nonlinear Waves" ed. by A.V. Gaponov-Grekhov, Moscow: Nauka. C. 131-163. 1979.

4. *Kaplan S.A., Tsytovich V.N.* Plasma Astrophysics. Series: Problems of Theoretical Astrophysics. Moscow: Nauka. 440 c. 1972.

5. *Landau L.D., Lifshits E.M.* Theoretical Physics. Vol. 8. Electrodynamics of Continuous Media. Moscow: Nauka. 621 c. 1982.

6. *Bakunina I.A., Melnikov V. F., Shain A.V., Kuznetsov S.A., Abramov-Maximov V.E..* Spatial Position of Magnetic Flux Ropes in Flare Active Regions with and without Coronal Mass Ejections

// Geomagnetism and Aeronomy. V. 64. № 8. P. 1237-1249. 2024. doi.org/10.1134/S0016793224700336

7. *Chen, B., Shen, C., Gary, D. et al.* Microwave Spectral Imaging of an Erupting Magnetic Flux Rope During a Large Solar Flare // Nature Astronomy. V.4. P. 1140-1147. 2020. doi.org/10.1038/s41550-020-1147-7

8. *Fleishman G.D., Gary D.E., Chen B., Kurod N., Yu S., Nita G.M.* Decay of the coronal magnetic field can release sufficient energy to power a solar flare // Science. V. 367. P. 278-280. 2020. doi.org/10.1126/science.aax6874

9. *Fleishman G.D., Nita G.M., Chen B., Yu S. and Gary D.E.*. Solar flare accelerates nearly all electrons in a large coronal volume // Nature. V. 606. P. 674-677. 2022. doi.org/10.1038/s41586-022-04728-8

10. *Ji H., Wang H., Schmahl E.J., Moon Y.J, Jiang Y.* Observations of the failed eruptions of the filament // Ap. J. V. 595. P. L135-L138. 2003doi.org/10.1086/378178

11. *Melnikov V.F., Meshalkina N.S.* Contraction Effect of Coronal Loops during the Flare of February 24, 2023 // Geomagnetism and Aeronomy. V. 64. № 8. P. 1381-1385. 2024. doi.org/10.1134/S001679322470052X

12. *Parker E. N.* Cosmical Magnetic Fields. Part 1. Oxford: Clarendon Press. P. 858. 1979.

13. Priest *E.* Solar Magnetohydrodynamics. Reidel Publishing Company. P. 469. 1982.

14. Priest *E., Forbes T.* Magnetic reconnection. MHD theory and applications. Cambridge, UK: Cambridge university press. 2000doi.org/10.1017/CBO9780511525087

15. *Solov'ev A.A., Kirichek E.A.* Force free magnetic flux ropes: inner structure and basic properties // MNRAS. V. 505. P. 4406-4416. 2021. doi.org/10.1093/mnras/stab1565

16. *Solov'ev A.A.* Force free magnetic flux ropes: string confinement of super-strong magnetic fields and flare energy release // MNRAS. V. 515. P. 4981-4989. 2022. doi.org/10.1093/mnras/stac1818

17. *Solov'ev A.A., Kirichek E.A.* Properties of flare energy release in force free magnetic flux ropes // Astronomy Letters. V. 49. № 5. P. 257-269. 2023doi.org/10.1134/S1063773723050055

18. *Solov'ev A.A., Korolkova O.A., Kirichek E.A.* Magnetic flux ropes on the Sun: electric currents and flare activity // Geomagnetism and Aeronomy. V. 63. № 8. P. 1120-1135. 2023. https://doi.org/10.1134/S0016793223080200

19. *Solov'ev A.A.* Force Free Magnetic Flux Rope with a High Current Density on the Axis // Astronomy Reports. V. 101. № 6. P. 601-609. 2024. doi.org/10.1134/S1063772924700550

20. *Solov'ev A.A., Murawski K.* Does the region of flare-energy release work as a vacuum-cleaner? // Astrophys. andd Space Sci. 2014. V. 350. P. 11-19. 2014. doi.org/10.1007/S10509-013-1716-7

21. *Wang H., Cao W., Liu Ch., Xu Y., Liu R., Zeng Zh., Chae J., Ji H.* Witnessing magnetic twist with high-resolution observation from the 1.6-m New Solar Telescope // Nature Communications. V. 6: 7008. 2015. doi.org/10.1038/ncomms8008

Figure captions

Fig. 1. A section of shielded magnetic harness of radius *a is* depicted , the current (large arrows) changes sign at a distance r_0 from the axis, so that . $I = \int_0^a 2\pi r \frac{1}{r}\frac{\partial}{\partial r}(rB_\varphi)dr = 2\pi\, rB_\varphi\Big|_0^a = 0$

(*a*) Tourniquet with strong current on the axis. (*b*) Tourniquet with peripheral current sheath.

Fig. 2. Function (10). The dotted line is the longitudinal field at G =2.5, the solid line is G = Gcr =2.0. Separately, the arrow shows the azimuthal field . $B_\varphi(kr)$

Fig. 3. For function (8) - A_1 - the azimuthal field $B_\varphi(kr)$ and the longitudinal current $j_z(kr)$, which changes sign when kr = 1, are shown.

Fig. 4. Flow function (dashed line) and longitudinal current distribution (solid line) in model 2 for different values of parameter *m*.

Fig. 5. Longitudinal magnetic field at *m* = 2 (second model) and different G. The solid line is G = $G_{crit} = 3.1974$, the dashed line is G = 2 G_{crit} . The dashed line is the azimuthal field.

Fig. 6. Cross-section of the harness for the case when the field direction at the lower circumference of the harness coincides with the direction of the external transverse field. The external force is directed upward.

Fig. 7. The direction of the external transverse field coincides with the direction of the azimuthal field on the upper bypass. A magnetic dome is formed, preventing the harness from lifting.

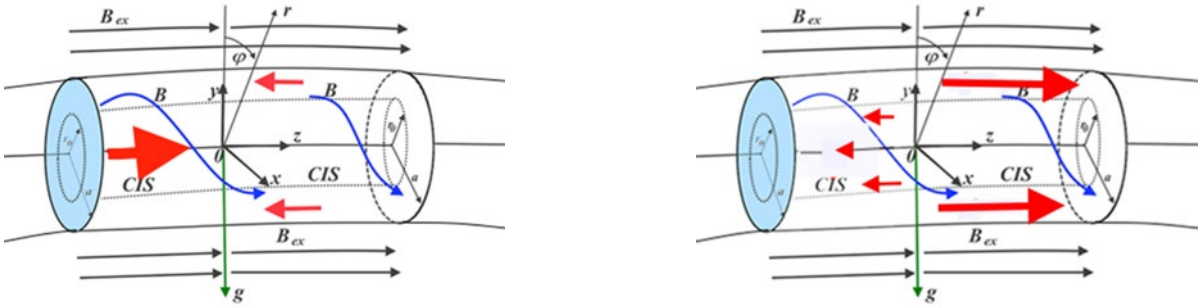

a *b*

Fig. 1

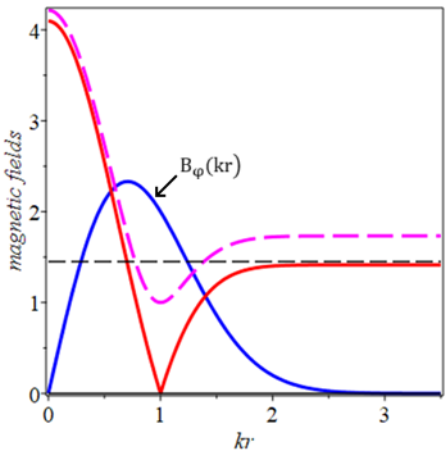

Fig. 2.

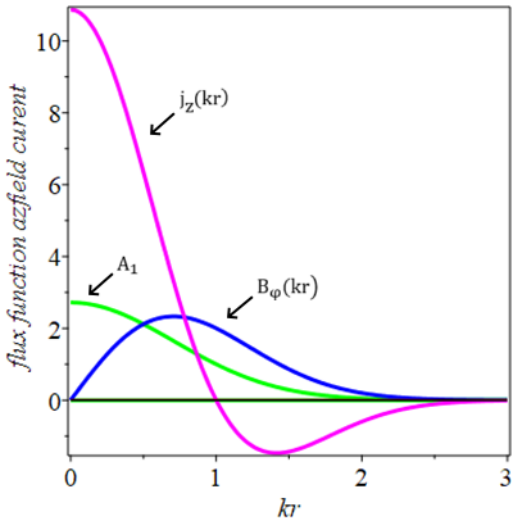
flux function azfield curent
10
8
6
4
2
0
0
1
2
3
kr
$j_z(kr)$
A_1
$B_\varphi(kr)$

Fig. 3.

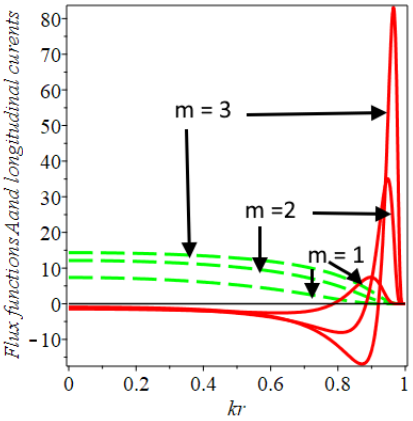
Flux functions A and longitudinal currents
80
70
60
50
40
30
20
10
0
-10
0
0.2
0.4
0.6
0.8
1
kr
m = 3
m =2
m = 1

Fig. 4.

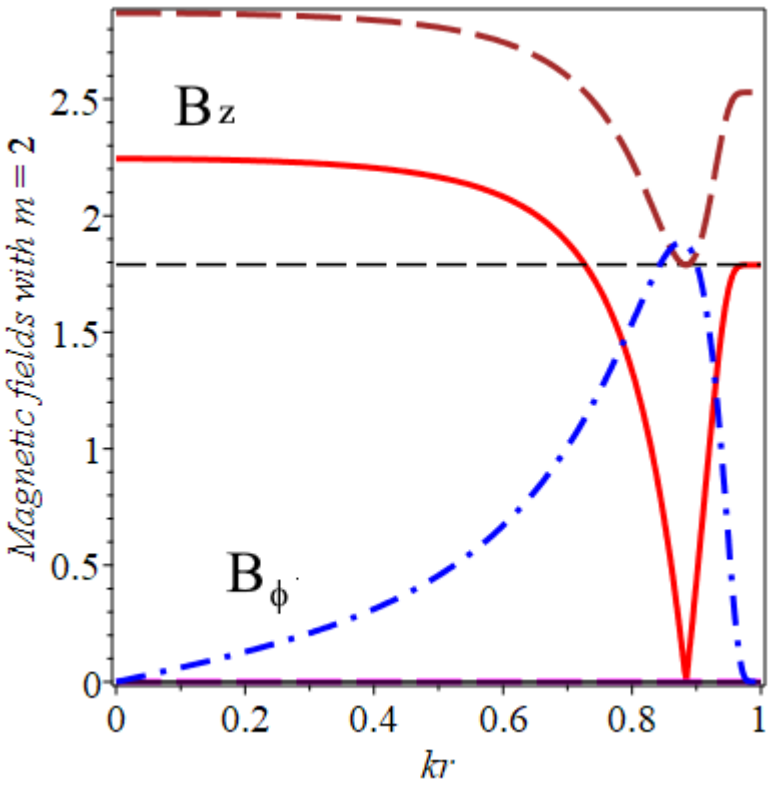

Fig. 5.

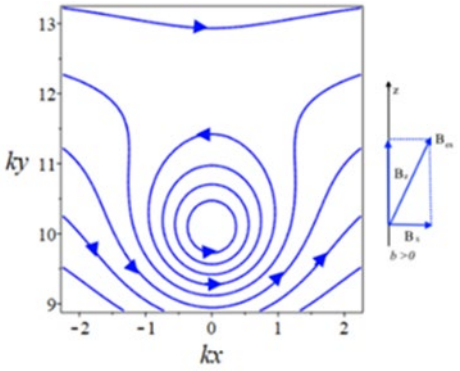

Fig. 6.

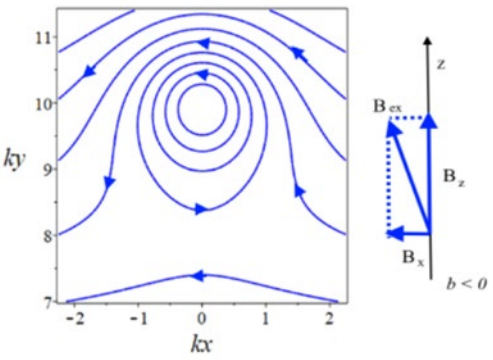

Fig. 7.